



# 3D concrete printing of eco-friendly geopolymer containing brick waste

Kirubajiny Pasupathy<sup>\*</sup>, Sayanthan Ramakrishnan, Jay Sanjayan

Centre for Sustainable Infrastructure and Digital Construction, School of Engineering, Swinburne University of Technology, Hawthorn, Victoria, 3122, Australia

## ARTICLE INFO

### Keywords:

Geopolymer concrete  
Digital construction  
Brick waste  
Rheological properties  
Porosity  
Compressive strength

## ABSTRACT

This study investigates alkali-activated brick waste powder as the binder for developing 3D printable geopolymer mixes. The brick waste was used as a partial replacement to fly ash in geopolymer binders. The effect of brick waste content on the fresh properties of printable mixes, such as flow, setting time and rheological properties were investigated. Besides, the hardened properties of 3D printed brick waste geopolymer were evaluated with the varying brick waste content in the mix. The test results demonstrated that the fresh properties of 3D printable mixes were improved with the brick waste content in the mix. Compared to the control mix, the mixes containing brick waste displayed high yield strength and apparent viscosity at an early age. On the contrary, the hardened properties of compressive strength and interlayer strength of 3D printed concrete specimens were decreased with the high brick waste content; however, the incorporation of brick waste for up to 10% has enhanced the hardened properties. Finally, the sustainability assessment of brick waste geopolymer studied with embodied energy and carbon emission calculations reveals the proposed geopolymer concrete could reduce the embodied energy and carbon emission by up to 60–80%, compared to OPC concrete.

## 1. Introduction

3D concrete printing (3DCP) has become a disruptive technology for the digital transformation of the construction industry due to its inherent advantages of formwork-free construction, fewer labour requirements, reduced construction-related accidents and enabling architectural freedom to construct artistically intricate structures [1]. The global construction trend also reveals that the construction industry has gradually gained momentum in transforming towards implementing digital construction technologies. In fact, some countries have already adopted 3DCP in the construction industry and some large-scale structures were built using 3DCP. The prominent examples can be listed as an office building in Dubai by WinSun [2,3], a house built by Apis Cor [4], full-scale bridges constructed in the Netherlands and the Hebei University of Technology, China [5]. On the other hand, global waste generation has increased massively in recent decades due to increasing population, rapid urbanization and developments of infrastructures. According to the statistical analysis, global waste production will be doubled by 2050, compared to the waste generated in 2016 and this will be expected to become triple by 2100 [6]. Although the recycling of waste materials into value-added products has been persuaded worldwide, huge quantities of waste materials are still sent to landfill sites. The disposal of waste on valuable lands is a serious concern as it is

causing significant environmental concerns including, land and resource depletion, contamination of soil, water and air and also affecting human health [6].

Among the different waste streams, construction and demolition (C&D) waste are one of the leading threats to the environment, since it is contributing to a large proportion of landfill waste. For example, the Australian C&D sector has contributed to around 44% of total solid waste generated in 2019 [7]. In recent years, Australia is one of the leading countries in waste recycling and it has already taken many steps in waste management technologies. Thus, the total recycling rate in Australia has increased to 60% in 2019, compared to 7% of the recycling rate in 1996 [8]. In C&D waste, masonry waste (i.e., concrete, bricks, asphalt, etc) is the major proportion representing about 85% of total C&D waste production [8]. Approximately 82% of masonry waste is recycled for many aspects, while the remaining 18% is still disposed to landfills [8]. The concrete from C&D waste is utilized for many applications including recycled concrete aggregates, road and pavement bases, pipe bedding, backfilling trenches, walls and drainage. However, the recovery of brick waste is very minimal, and only a small proportion of brick waste is utilized for garden bed toppings, driveways, and landscaping. Therefore, converting brick waste into valuable resources can be a potential solution to divert the C&D waste generated by bricks.

At present, significant research studies have been conducted on the

<sup>\*</sup> Corresponding author.

E-mail address: [kpasupathy@swin.edu.au](mailto:kpasupathy@swin.edu.au) (K. Pasupathy).

use of brick waste as a partial replacement for aggregates in conventional concrete [9,10]. It has been reported that brick waste aggregates provide comparable performance to conventional concrete. On the other hand, brick waste has also been explored as a precursor for making geopolymer concrete. Geopolymer concrete is a sustainable alternative to Portland cement-based concrete by replacing cement with industrial wastes [11]. Geopolymer concrete is generally formulated by alkali activation of silica ( $\text{SiO}_2$ ) and alumina ( $\text{Al}_2\text{O}_3$ ) rich sources in the presence of other constituents such as aggregates and admixtures. The most widely studied silica and alumina-rich sources for geopolymerization are fly ash, slag, meta kaolin, etc. However, it must be stressed that recent technological advancements have led to an increase in the fly ash utilization rate in concrete [12] and the fly ash reserve is rapidly depleting in many countries, including Australia [13]. In this regard, the exploration of other waste byproducts that are rich in silica and alumina is essential.

Ground brick waste possesses high proportions of  $\text{Al}_2\text{O}_3$  and  $\text{SiO}_2$  components and it has been classified as a low-amorphous precursor material for formulating geopolymer binder [14]. Compared to other precursor materials (fly ash or slag), the geopolymerization reaction is slow at ambient temperature due to the low levels of amorphous content in ground brick [15]. Therefore, ambient temperature cured brick powder-based geopolymer possesses a limited compressive strength such as 10.2 MPa at 14 days [15]. In contrast, elevated temperature curing has been found to significantly enhance the strength development in brick waste geopolymer concrete. For instance, Wong et al. [14] have achieved a compressive strength of up to 36.2 MPa after being subjected to elevated temperature curing at 90 °C for 5 days. In another study, it was reported that the brick waste geopolymer concrete displayed a compressive strength of up to 30–50 MPa when it was subjected to curing at 65 °C for 7 days [16]. More recently, ground brick waste was also used to develop lightweight geopolymer concrete with a density of 700 kg/m<sup>3</sup> [17,18]. Although the activation of brick waste requires an elevated temperature curing process, the brick waste has potential benefits when it is considered in the geopolymer concrete preparation. Besides, the elevated temperature curing could be avoided by introducing high amorphous precursors (such as slag or fly ash) at a partial replacement in geopolymer concrete. More recently, Migunthanna et al. [19] investigated the possibility of waste clay brick as a partial replacement of geopolymer binders for rigid pavement application and reported that the partial replacement of brick waste geopolymer showed compressive strength above 40 MPa when it was cured at ambient temperature. On the other hand, ground brick waste was also used to replace Portland cement due to its pozzolanic nature. Past studies revealed that 10%–20% of cement replacement with ground brick waste provides similar or higher compressive strength than Portland cement concrete [20–22]. Moreover, Zhao et al. [23] studied the environmental impact and carbon footprint assessment of the replacement of cement with ground brick waste. The analysis showed 30% of brick waste replacement reduces CO<sub>2</sub> emission by up to 70.9% compared to Portland cement concrete. Therefore, it can be understood that there is a promising pathway to utilize brick waste in concrete production that will benefit from reducing waste generation as well as alleviating the consumption of high energy-intensive Portland cement.

3DCP primarily uses extrusion technology, where a precise amount of materials is extruded and deposited through a nozzle to construct a layer-by-layer structure. In contrast to the traditional construction methods, the 3DCP method does not use formwork or lateral support during the construction process. Due to the absence of formwork and lateral support, the concrete needs to develop sufficient early-age strength during its placement to retain the shape of the structure and to avoid significant deformations or collapse of the structure. The ability of the concrete to meet this requirement is known as buildability [24]. Meanwhile, the concrete needs to be flowable during the pumping process for ease of pumping. Therefore, the early-age rheological properties of printable concrete are crucial to achieving

high-performance 3D printed structures. An extensive review of the application of 3D printing in concrete, printing methods, fresh and hardened properties of 3D printing concrete and the potential benefits of 3D printing in the construction industry can be found elsewhere [25–27]. The use of various recycled materials as a partial replacement for fine aggregates in 3D printable concrete is also studied. For instance, recycled concrete as fine aggregate [28] or coarse aggregates [29], waste glass [30] and ground waste tyres [31] were studied to make 3D printable concrete.

In light of the brick waste geopolymer concrete, past studies reveal that the incorporation of ground brick waste affects the early age rheological properties of the geopolymer mix. Rovnaník et al. [15] observed that the plastic viscosity and the thixotropy of geopolymer mixes were decreased with the addition of brick waste due to the low amorphous content and corresponding slow reaction rates of geopolymerization. In contrast, Duan et al. [32] found that the yield stress, plastic viscosity and thixotropy of fresh mixes are increased with the addition of brick waste. However, whether the corresponding increase in the yield stress and thixotropy is sufficient to improve the buildability of 3D-printed structures is yet to be explored.

This study investigates the potential of using ground brick waste as a precursor for the emerging construction technology of 3D concrete printing (3DCP). Four different 3D printable geopolymer concrete mixes were prepared with varying proportions of ground brick waste. The rheological behaviour of fresh 3D printable mixes, including the static yield stress and viscosity, were analysed and compared. Moreover, the hardened properties including the compressive strength at three directions, interlayer bond strength and porosity were determined and compared with the 3D printing geopolymer concrete prepared without brick waste powder. In addition, the microstructure characterization was also evaluated. Finally, embodied carbon emissions and energy consumption of the developed 3D printable geopolymer concrete mixes were calculated and compared with the traditional 3D printable concrete mix to assess the environmental impacts and carbon footprints.

## 2. Methodology

### 2.1. Materials

The ground granulated blast furnace slag (GGBFS), low-calcium fly ash (class F) and ground brick waste are used at different proportions to formulate the geopolymer binder. The fly ash and GGBFS were supplied by Cement Australia, and Independent Cement and Lime Pty Ltd., Australia, respectively. Both materials comply with Australian standard AS 3582.1 [33]. The brick waste used in this study was purchased from Eco Group, Australia. The maximum particle size of the supplied brick waste was 1.1 mm. Therefore, it was ground before being used as a precursor material for the geopolymer binder formulation. To conduct the grinding process, the brick waste was first oven-dried at 105 °C for 24 h to remove any moisture and then powdered by using the ball mill. Thereafter, the fine powder was sieved through a 75 µm standard sieve and used as a precursor material for geopolymer formulation. The chemical composition of brick waste powder, determined by X-Ray Fluorescence (XRF) analysis, is shown in Table 1. The particle size distribution of ground brick waste was determined by a dual light source laser diffraction particle size analyser, and the cumulative passing volumes are shown in Fig. 1. According to the results, the median diameter (D50) of the brick waste powder was determined as 20.5 µm. For the activation process, sodium metasilicate ( $\text{Na}_2\text{SiO}_3$ ) anhydrous powder ( $\text{SiO}_2/\text{Na}_2\text{O} = 1.0$ ), purchased from Redox Pty Ltd, Australia, was used as a sole one-part activator.

Two different types of silica sand with different sizes such as coarse and fine sand was used for the preparation of 3D printable geopolymer concrete. The median diameter (D50) of the fine and coarse sand were 172 µm and 498 µm, respectively. A small dosage of sucrose powder was used as the retarder to increase the open time of the geopolymer mixes.

**Table 1**  
Chemical composition of BW powder determined by XRF (reproduced from Ref. [17]).

	SiO <sub>2</sub> (%)	Al <sub>2</sub> O <sub>3</sub> (%)	CaO (%)	Fe <sub>2</sub> O <sub>3</sub> (%)	K <sub>2</sub> O (%)	SO <sub>4</sub> (%)	TiO <sub>2</sub> (%)	MnO (%)	LOI <sup>a</sup> (%)
Ground Brick waste	68.4	8.5	3.9	12.0	4.7	0.3	1.7	0.1	0.4

<sup>a</sup> LOI means loss on ignition at 1000 °C.

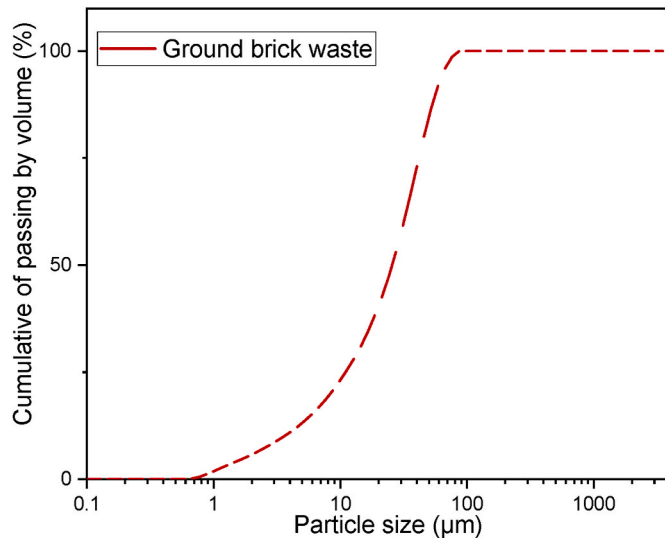


**Fig. 1.** Particle size distributions of ground brick waste (reproduced from Ref. [17]).

It should be noted that sucrose powder is identified as the best retarder for the one-part geopolymer mix [34,35]. Moreover, Nano clay supplied by Active Minerals International, LLC was used as a thixotropic modifier in this study.

## 2.2. Sample preparation

The mixture proportions of the materials used to prepare different types of 3D printable geopolymer are reported in Table 2. The ground brick waste was incorporated as a partial replacement to fly ash at the proportion of 10%, 30% and 50% of the precursor in the mixes of M<sub>2</sub>, M<sub>3</sub> and M<sub>4</sub>, respectively. Here, the total precursor content was kept constant in all the mixes. In addition, the mass ratio between total sand and precursor materials was kept constant at 1.5. The solid sodium metasilicate anhydrous (Na<sub>2</sub>SiO<sub>3</sub>) activator with 10% of precursor weight was used for all mixtures. This is the optimum dosage of solid activator for the synthesis of one-part geopolymer, as observed by past researchers [36,37]. Moreover, the thixotropic additive was used at 0.5% of precursor weight in all the mixes, to enhance the thixotropic behaviour of the mixes. The required dosages of nano clay and retarder were obtained from past studies [35,36] and via a trial and error approach. It should be noted that, except for the precursor materials, the remaining components were kept constant in all mixes to study the effect of the incorporation of brick waste powder in the 3D printable geopolymer concrete.

The mixing procedure was as follows: Initially, all the dry ingredients

were added in a Hobart mixer and mixed for 3 min at a low speed to ensure homogeneous dispersion of the dry materials. Thereafter, 85% of the total water was added and the mixing was continued for another 10 min at medium speed. After that, the remaining amount of water was added to the mix and the mixing was continued for another 5 min to avoid the workability loss of mix due to the dissolution of the activator as reported in previous studies [35]. Similar mixing duration was also followed by Bong et al. [38] and Muthukrishnan et al. [35] for the preparation of one-part geopolymer concrete for 3D printing. This is mainly to allow enough time to ensure the complete dissolution of the solid metasilicate activator throughout the mixing process.

## 2.3. 3D printing process

Fig. 2 (a) illustrates the three-axis gantry type 3D printer used for printing the geopolymer specimens. The maximum printing space of the printer is 1800 mm (L) × 1600 mm (W) × 1800 mm (H). An auger extruder was attached to the 3-axis rail system and the movement of the extruder was navigated by a customized computer program in the printer software interface. The materials are fed from the top part of the hopper and the diameter of the circular outlet of the extruder was 30 mm. Fig. 2 (c) shows the printing process of the brick waste geopolymer used in this study. During the printing process, the printing speed was kept at 10 mm/s for all mixtures. The samples were printed with the dimensions of each layer at 30 mm (W) × 20 mm (H) × 300 mm (L). The printed samples were covered with plastic film to eliminate the moisture loss from the surface and to avoid crack formation on the surface. After 24 h, the samples were removed from the printing platform and subjected to the heat curing process for 24 h at 60 °C temperature. In addition, 50 × 50 × 50 mm<sup>3</sup> cube specimens were also prepared for the comparison of properties with cast specimens. It should be noted that the elevated temperature curing method was adopted here to enhance the reaction rate of low amorphous brick waste powder. Moreover, the heat curing process was also widely used for the 3D printed samples by past researchers to enhance the strength properties of the 3D printed elements [39]. After 24 h of curing at elevated temperatures, the samples were kept in a sealed container at the ambient temperature until the test date.

## 3. Experimental programme

### 3.1. Fresh stage properties

#### 3.1.1. Flow measurements of fresh mix

The two primary contradicting requirements of 3D printable concrete mixtures are buildability and pumpability and they are related to the fresh properties. Past research has reported that the slump measurement of the fresh mix can be used to evaluate the static yield stress and buildability, while the slump flow measurement can be related to

**Table 2**  
Mix compositions of 3D print concrete.

Mix No	Slag (g)	Fly ash (g)	Ground brick waste (g)	Coarse sand (g)	Fine sand (g)	Sodium Metasilicate (g)	Water (g)	Retarder (% of precursor)	Nano clay (% of precursor)
M <sub>1</sub>	500	500	–	1000	500	100	400	1.0	0.5
M <sub>2</sub>	500	400	100	1000	500	100	400	1.0	0.5
M <sub>3</sub>	500	200	300	1000	500	100	400	1.0	0.5
M <sub>4</sub>	500	–	500	1000	500	100	400	1.0	0.5

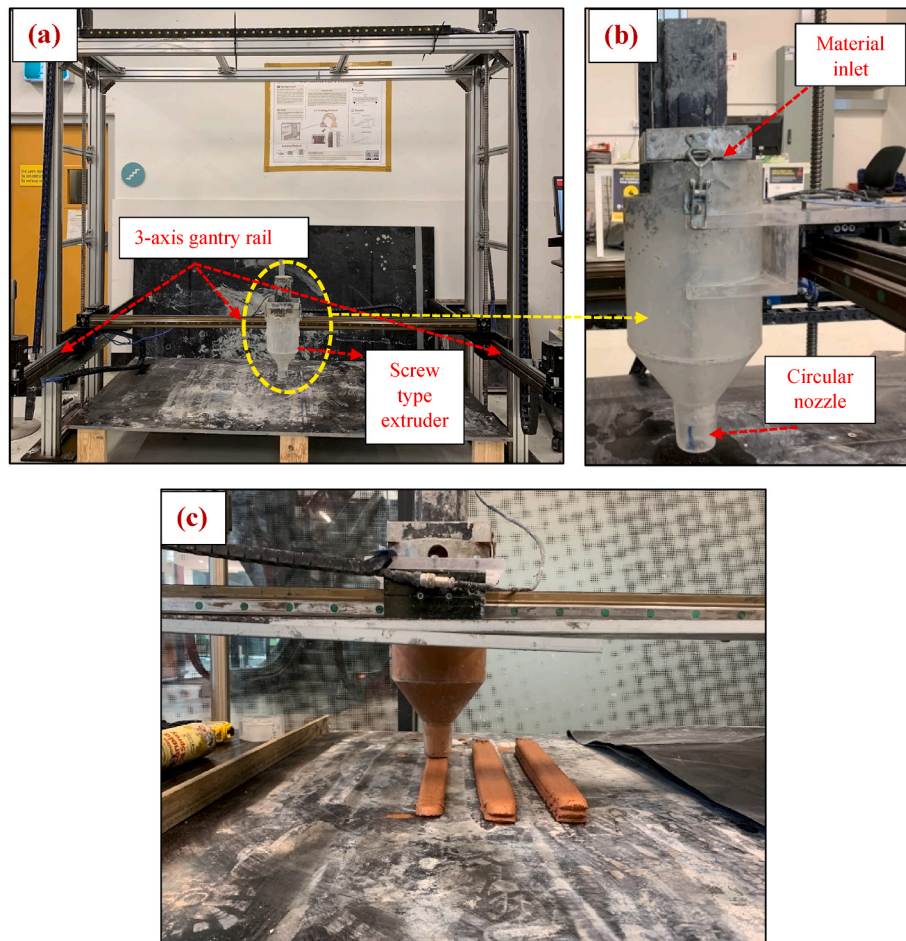


Fig. 2. (a) Diagram of gantry type 3D printer used for this study (b) Extruder, (c) Printing process.

the dynamic yield stress and pumpability of the 3D printable mixes [40]. Therefore, the flow measurements of the fresh mixes were determined according to the ASTM C1437 [41] standard using a flow table apparatus. The testing procedure was as follows: The fresh mortar mix was filled as two layers in a mini-slump cone with the dimension of top and bottom diameters of 70 mm and 100 mm and a height of 60 mm. Each layer was tamped 20 times using a tamping rod. Once the two layers are filled and compacted, the excess mortar was removed by a straight edge so that the concrete surface is flushed with the cone. The cone was lifted, and the diameter of the fresh mix was measured at two orthogonal directions to derive the average spread diameter. Thereafter, the flow table was dropped 25 times and the final diameter of the flow was determined in two perpendicular directions. The average of two values was reported as the final slump flow readings.

### 3.1.2. Rheological properties of the fresh mix

To determine the rheological properties of fresh mixes, a rotational rheometer (Viskomat XL) with a six-blade vane probe was employed. The radius and the height of each blade were equal to 34.5 mm and 69 mm, respectively. It is worth mentioning here that the vane probe was designed to determine the rheological parameters of cementitious materials with a maximum particle size of 20 mm. The radius of the vessel used for filling the fresh concrete was 82.5 mm.

The nature of 3DCP generally involves initial high shearing at the mixing stage, followed by low shearing at pumping, then high shearing during the extrusion followed by placement. For shear-thinning materials like concrete, the apparent viscosity drops from a significantly higher value to a low value when the mix is transformed from a low shear rate to a high shear rate. Therefore, it is important to ensure that

the concrete recovers its viscosity after a high-shearing event followed by low shearing. To assess this phenomenon, a viscosity recovery test is generally performed. The viscosity recovery of fresh concrete mixes was evaluated in accordance with the method used in Refs. [24,42]. Fig. 3 illustrates the shearing protocol used for the viscosity recovery measurement. As shown in Fig. 3, the apparent viscosity values were

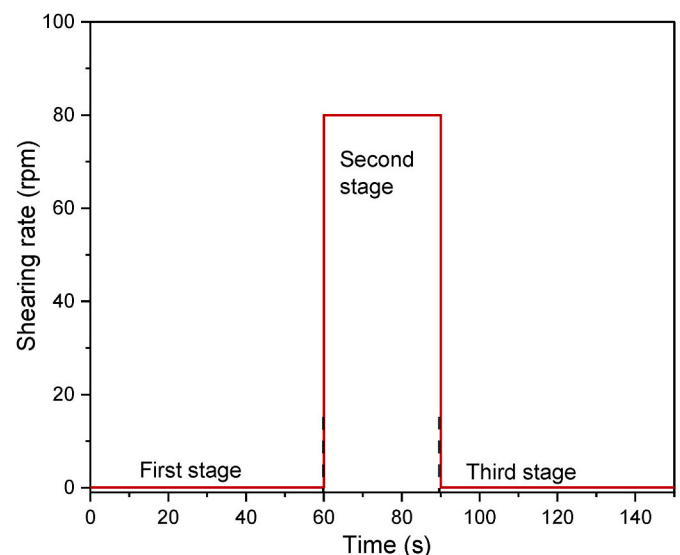


Fig. 3. Rheological testing protocols for viscosity recovery measurements.

determined in three stages to evaluate the recovery rate. During the first stage, the mix was sheared at a constant shear rate of 0.1 rpm for 60 s to simulate the rest time behaviour of the mix before printing. During the second stage, the mix was sheared at the maximum rate of 80 rpm to represent the printing stage such as extrusion. Then the mix was sheared at the rate of 0.1 rpm for 60 s to simulate the placement of the mix after the extrusion, which is representing the shape retention behaviour of the mix. It should be noted that, before starting the test, the mixture was pre-sheared at 80 rpm for 60 s to ensure the starting point is the same for all measurements.

The static yield stress of the fresh mix was measured using the constant shear rate protocol as shown in Fig. 4 (a). The static yield stress plays an important role in the buildability of the 3D printing processes. During the testing procedure, the fresh mix was deflocculated by pre-shearing at 80 rpm for 60 s to ensure a uniform starting point for all the tests. After that, the mix was kept rest for another 60s and then it was sheared at a constant shear rate of 0.1 rpm for 60 s to determine the static yield stress properties.

### 3.1.3. Setting time measurement of the fresh mix

Since the brick waste powder is a low amorphous precursor material, the setting time measurements of fresh geopolymer mixes were determined to evaluate the reaction rate with the addition of brick waste in 3D printable mixes. The initial and final setting time of the fresh paste mixes (without sand) was determined according to ASTM C191 [43] by using a Vicat needle apparatus.

## 3.2. Hardened properties

### 3.2.1. Compressive strength measurements

The compressive strength measurements were determined on the samples extracted from 3D printed filaments and the strength values were measured in three different directions of longitudinal, lateral and perpendicular directions to assess the anisotropic behaviour of 3D printed samples. Fig. 5 illustrates the schematic diagram of the compressive strength test specimens extracted from printed samples in three testing directions. The tests were performed on the cube specimens with the size of  $30 \times 30 \times 30 \text{ mm}^3$  at the age of 7 days and 28 days. For compressive strength testing, a Universal Mechanical Testing System (MTS) with a maximum load capacity and precision of 300 kN and 0.01 kN respectively was used. Three designated samples were used for testing in each direction and the average and standard deviation of the three samples were reported. Besides, the compressive strength of 3D printing filaments was compared with the compressive strength of the mold cast specimen. The compressive strength of  $50 \times 50 \times 50 \text{ mm}^3$  mold cast specimens was determined at 28 days period at the same loading rate.

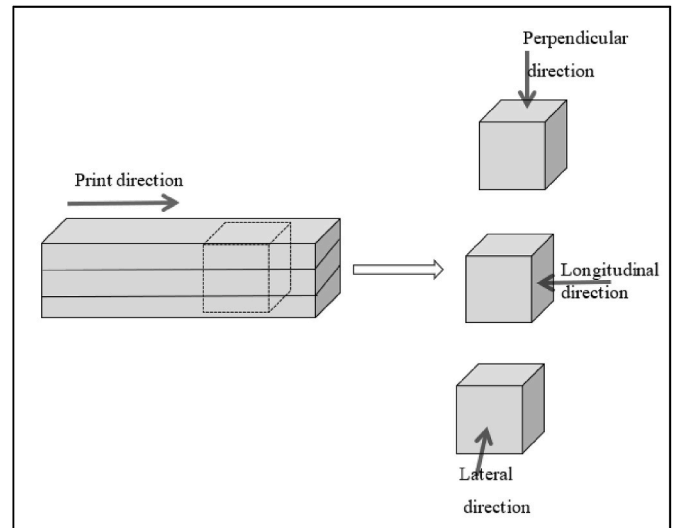


Fig. 5. Schematic diagram of samples extracted from printed samples and testing directions of compressive strength tests.

### 3.2.2. Interlayer bond strength measurements

For the interlayer bond strength test,  $30 \times 30 \times 40 \text{ mm}^3$  specimens were extracted from  $300 \times 30 \times 40 \text{ mm}^3$  printed samples on the test date. The test setup used for the interlayer bond strength measurements is shown in Fig. 6. As shown, the sample was clamped using metallic brackets at the top and bottom and the tapered claws of the metallic brackets were aligned at the interlayer of the samples to ensure the uniform stress distribution at the interlayer. The test was performed using an MTS machine at the displacement control mode of 1 mm/min. A small notch with a size of 4 mm was prepared at the interlayer of the samples to make sure the failure occurs at the interface of the 3D-printed filaments. The same setup was also used in past research studies to measure the interlayer bond strength of 3D-printed elements [42,44].

### 3.2.3. Physical properties measurements

The physical properties such as bulk density and apparent porosity of 3D printed concrete were determined by following the ASTM C830 standard. To conduct the test,  $30 \times 30 \times 30 \text{ mm}^3$  size samples were extracted from the 3D printed filaments and the samples were first oven-dried at  $105^\circ \text{C}$  for 24 h. After 24 h, the weight of the samples was determined (D in g). Thereafter, the samples were immersed in water for saturation in a vacuum pressure vessel for 24 h and the weight of the saturated samples was measured (W in g). Then, the saturated samples were used to determine the suspended weight and the suspended weight values were recorded as S in g. The precision of the digital balance used for the weight measurements was 0.01 g. The bulk density (B in  $\text{kg/m}^3$ )

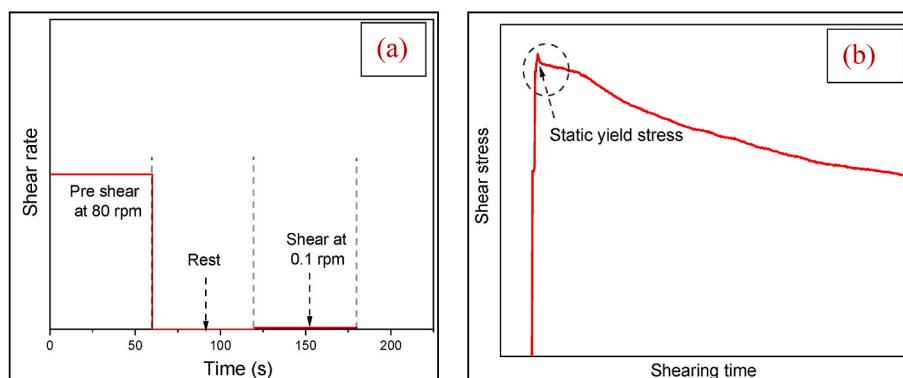


Fig. 4. (a) Rheological testing protocols for static yield stress measurements, (b) Typical hysteresis curve for static yield stress measurement.

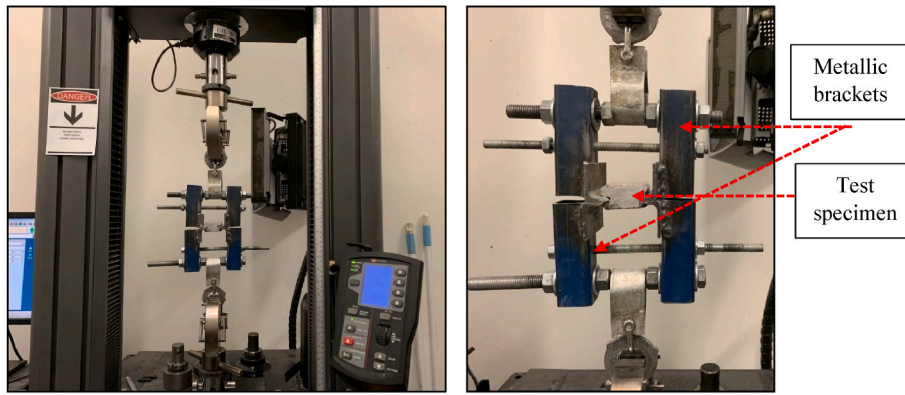


Fig. 6. Interlayer bond strength measurement.

and apparent porosity (P, %) were calculated using the following equations:

$$B = \frac{D}{W - S} \times 1000 \tag{1}$$

$$P = \frac{W - D}{W - S} \times 100\% \tag{2}$$

3.3. Micro-morphology analysis at the interlayer

To understand the influence of the brick waste powder on the geopolymer reaction product, a scanning electron microscopy (SEM ZEISS Supra 40 VP) analysis was conducted on the samples collected from the printed filaments. To perform the test, a 10 mm size sample was extracted from 3D printed samples after 28 days of printing and the samples were first gold-coated at 15 nm coating using a K975X vacuum coating system. The SEM images were processed at an accelerated voltage of 5 kV and a working distance (WD) of 20–27 mm.

4. Results and discussion

4.1. Fresh state properties

4.1.1. Flow and setting time measurements

The test results of slump-flow measurements of fresh geopolymer concrete mixes before and after dropping the flow table are presented in Table 3. In addition, the setting time measured by using the Vicat needle penetration test is also provided in Table 3. The test results indicated that the partial replacement of geopolymer precursors with brick waste powder displays high shape retention and good pumpability properties. The control mix without brick waste (M<sub>1</sub>) was chosen based on the optimum 3D printable geopolymer mix, which has ‘zero’ slump requirements. Therefore, the flow diameter measured before dropping the table for the mix M<sub>1</sub> was 100 mm, which indicates zero slumps (no flow after lifting the cone). Besides, all other types of mixes with the addition of brick waste also showed a spread diameter of 100 mm before drop the flow table, which indicates the zero slump in these mixes without the modification in the water-to-binder ratio. Therefore, this specifies that

Table 3  
Slump flow and setting time measurements of fresh 3D printable mixes.

Mix No	Flow properties		Setting time	
	Flow value-before drop (mm)	Flow value-after drop (mm)	Initial (min)	Final (min)
M <sub>1</sub>	100	152.5	102	145
M <sub>2</sub>	100	147.5	112	154
M <sub>3</sub>	100	140.5	120	159
M <sub>4</sub>	100	135.0	125	168

all mixes should exhibit excellent shape retention properties, regardless of the brick waste content in the geopolymer mix.

The slump–flow measurements conducted by dropping the flow table (25 times) show the variation in slump-flow diameter. As can be seen from Table 3, the increase in the brick waste content has resulted in the flowability loss of the fresh mix, where the flow diameters are decreased with the brick waste content in the mixes. Compared to the control mix (M<sub>1</sub>), the flow diameters of the M<sub>2</sub>, M<sub>3</sub> and M<sub>4</sub> mixes were reduced by 3.3%, 7.9% and 11.5%. This could be attributed to the loss of the ball-bearing effect due to the substitution of round and spherical fly ash particles with irregularly shaped brick particles [45]. Moreover, the brick waste powder possesses high water absorption characteristics and therefore the flowability is decreased with increasing brick waste content in the mix [45].

On the other hand, the setting time of the fresh mix is increased with the increasing brick waste content. This is primarily due to the low geopolymerization reaction rate of brick waste precursor, compared to fly ash precursor [17]. As shown in Table 3, both initial and final setting times of the M<sub>2</sub>, M<sub>3</sub>, and M<sub>4</sub> mixes were slightly higher than the control mix with 10–23 min for M<sub>2</sub>–M<sub>4</sub> mixes. Such increment in setting time is not expected to significantly affect the buildability of printed structures.

4.1.2. Rheological properties

The partial substitution of brick waste should ensure good viscosity recovery properties for its use as a 3D printable mix. The printable mixes with high viscosity recovery properties exhibit a high recovery to their original apparent viscosity when subjected to the proposed shearing

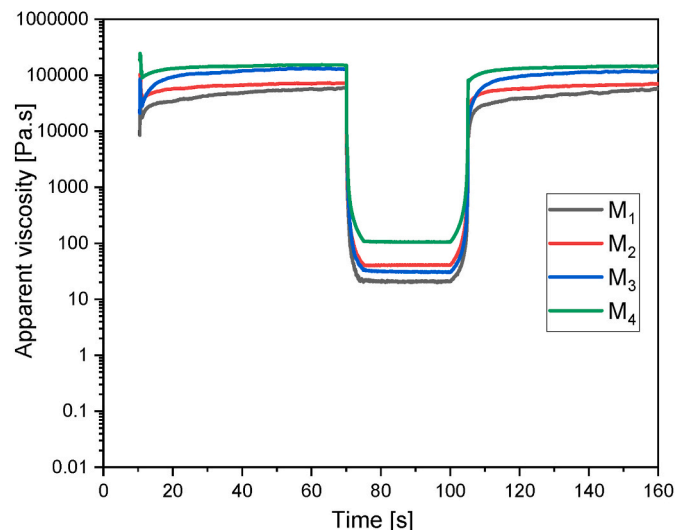


Fig. 7. Viscosity recovery of 3D printable mixes with brick waste.

protocol. Fig. 7 illustrates the apparent viscosity properties of the geopolymer mixes for the proposed shearing protocol with varying brick waste content. Here, the viscosity measurements are divided into three stages; stage 1 represents the rest period before extrusion, where high viscosity is reported. In stage 2, the mix becomes flowable with lower viscosity, which indicates the extrusion stage and stage 3 has a high viscosity which represents the placement state after extrusion. From Fig. 7, an excellent viscosity recovery behaviour can be observed for all the mixes. It is also interesting to note that the recovery ability is slightly improved with the brick waste content in the mix. Moreover, the apparent viscosity values also increased with the addition of brick waste when the mix was kept at rest. As can be seen from Fig. 7, the apparent viscosity values of the M<sub>1</sub> type mix were in the order of  $\sim 10^4$  Pa, whereas the mix with the highest brick waste content (M<sub>4</sub>) displayed the apparent viscosity in the order of  $\sim 10^5$  Pa. This indicates that the addition of brick waste enhances the re-flocculation ability which can improve the buildability characteristics during the printing process. Besides, the apparent viscosity at the high shearing stage (stage 2) shows that the incorporation of brick waste powder increases the viscosity. This observation is consistent with the slump flow measurement observed in Section 4.1.1, where the loss of the ball-bearing effect has caused the increased apparent viscosity.

Fig. 8 illustrates the comparison of the evolution of static yield stress with time for different geopolymer mixes. As can be seen, the static yield stress of geopolymer concrete is increased with the brick waste content in the mix. It is worth mentioning that the static yield stress is defined as the critical stress that is required to initiate the flow of the mix from the rest condition and the yield stress values are related to the free water content in the slurry, flocculation of the particles, and the reaction process [46,47]. Here, although the reaction rate of geopolymer mixes is reduced with the increasing brick waste content (i.e. increase in the setting time with brick waste), the incorporation of brick waste absorbs free water in the mix due to the irregular shape of brick particles [45]. Decreasing the free water in the mix accelerates the internal friction between the particles and increases the shear stress and viscosity [48]. As a result, the static yield stress is increased with the addition of brick waste in geopolymer.

Fig. 9 shows the laboratory scale 3D printing of brick waste geopolymer concrete structure using the developed 3D printable mixes. The mix M<sub>3</sub> was considered for 3D printing purposes using a gantry-type 3D printer. Approximately 20 layers were continuously printed without any interruption or discontinuity during the printing and the height of the printed structure was 300 mm. Therefore, this confirms the feasibility of

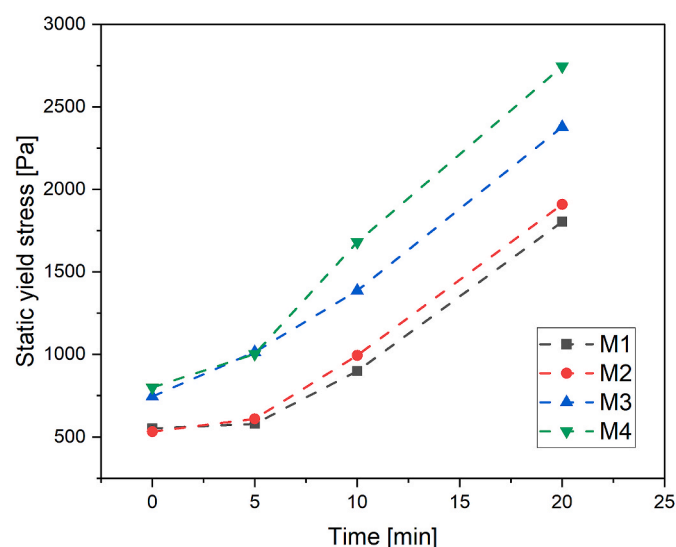


Fig. 8. The static yield stress of 3D printable mixes varying with time.

utilizing brick waste in the 3D concrete printing application, which promotes the recycling of waste in construction applications.

## 4.2. Hardened properties

### 4.2.1. Compressive strength of 3D printed concrete

Fig. 10 (a) and (b) illustrate the compressive strength test results of 3D printed geopolymer concrete filaments after 7 days and 28 days, respectively. The strength values of 3D printed specimens are measured in three directions of longitudinal, lateral and perpendicular directions. In addition, the 28 days' compressive strength of mold casting specimens is also included in Fig. 10 (b) to compare the strength variation due to the printing process. The error bar represents + or - one standard deviation from the average strength values. According to the test results, the M<sub>2</sub> type with 10% brick waste displayed the highest compressive strength regardless of the printing directions or mold casting. Compared to the M<sub>1</sub> type, the 28 days compressive strength of M<sub>2</sub> type printed specimens was increased by 2.9%, 3.8% and 12.4% in longitudinal, lateral and perpendicular directions, respectively. Similarly, the strength of mold cast specimens was increased by 10.8% after 28 days period. The increase in brick waste content above 10% of precursor has resulted in a decrease in compressive strength properties for 3D printed and mold-cast specimens. For example, the M<sub>4</sub> mold-cast specimens showed approximately an 8.6% drop in 28 days of compressive strength, compared to the control mix (M<sub>1</sub>). Meanwhile, the 3D-printed M<sub>4</sub> specimens showed a reduction of 21.2%, 14.6% and 27.8% of the 28 days of compressive strength in longitudinal, lateral and perpendicular directions respectively, compared to the M<sub>1</sub>. The reduction of strength is caused by the low amorphous content in brick waste resulting in a low reaction rate of the brick waste precursor [49]. Therefore, the strength properties are decreased with the increase in brick waste content in the mix. Nevertheless, the measured compressive strength properties are above 25 MPa at 28 days for all mixes, demonstrating the use for structural concrete purposes for many building applications, while benefiting from the recycling of C&D waste.

It can also be found that the compressive strength of mold casting specimens is higher than the compressive strength of printed specimens in all tested directions. This could be due to the formation of inherent voids during the printing process caused by the circular type nozzle used in the printing [50]. Therefore, the compressive strength of 3D printed specimens is lower than the mold cast specimens. Moreover, the anisotropic strength behaviours are portrayed for printed samples, where the strength values are varied with the testing directions. As can be seen in Fig. 10, the compressive strength in the longitudinal direction (printing direction) was found to be the highest in all mixes, and the least compressive strength properties are observed in the lateral direction. Similar compressive strength patterns were also reported by other researchers [42,51]. The high strength properties observed in the printing direction are due to the high compaction in the printing direction caused by the pressure from the extrusion process. In contrast, the lowest compressive strength in the lateral direction can be related to the presence of a weaker interlayer with increased porosity or voids between the adjacent printed layers [52,53].

### 4.2.2. Interlayer bond strength of 3D printed concrete

In 3DCP, the weakest plane was found to be at the interlayer leading to poor interlayer bond strength and low compressive strength in the lateral direction [54]. Therefore, it is important to determine the effect of brick waste addition on the interlayer bond strength of 3D-printed filaments. The interlayer bond strength results of 3D printed specimens with varying brick waste content are shown in Fig. 11. The error bar represents + or - one standard deviation from the average strength values. It should be noted that all specimens showed failure at the interlayer during the testing. From Fig. 11, it can be observed that the interlayer bond strength is decreased with the increasing brick waste content in the mix, except for the M<sub>2</sub> group of specimens with 10% of



Fig. 9. 3D printed structures using optimum mix (M<sub>3</sub>).

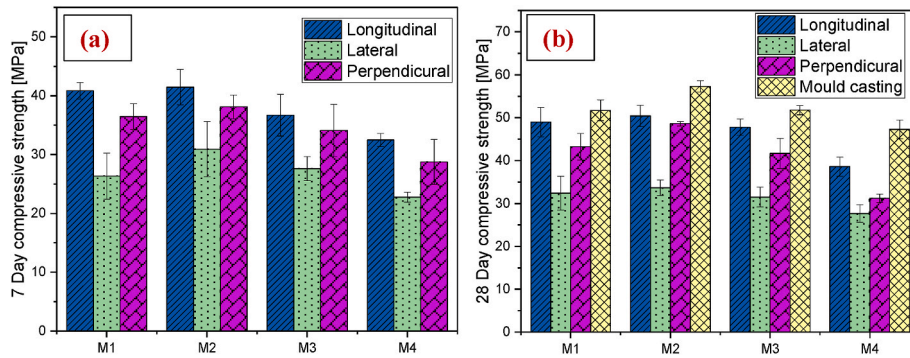


Fig. 10. (a) 7 Day compressive strength values; (b) 28 Day compressive strength values.

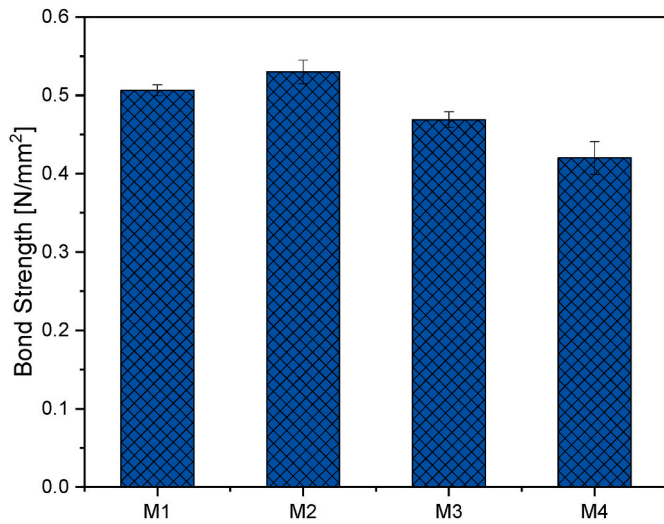


Fig. 11. Interlayer bond strength values of 3D printed samples.

brick waste precursors. This trend can be correlated with the compressive strength test results, where the compressive strength is increased for M<sub>2</sub> followed by a decrease for the subsequent groups. Compared to the control specimens (M<sub>1</sub> type), the interlayer bond strength of the M<sub>2</sub> is increased by 4.5%, whereas M<sub>3</sub> and M<sub>4</sub> are decreased by 7.4% and 16.8% respectively.

#### 4.2.3. Physical properties of 3D printed concrete

Fig. 12 demonstrates the bulk density and apparent porosity of 3D-printed concrete samples with varying brick waste content in the mix. The error bar represents + or - one standard deviation from the average strength values. In general, the apparent porosity values of 3D printed specimens are greater than the mold cast specimens due to the inevitable voids introduced between printed layers during the layer-by-layer extrusion process [55]. Studies have reported that 3D-printed concrete consists of a higher amount of macro-pores and irregular shapes of large voids [56]. According to the test results, the apparent porosity of 3D

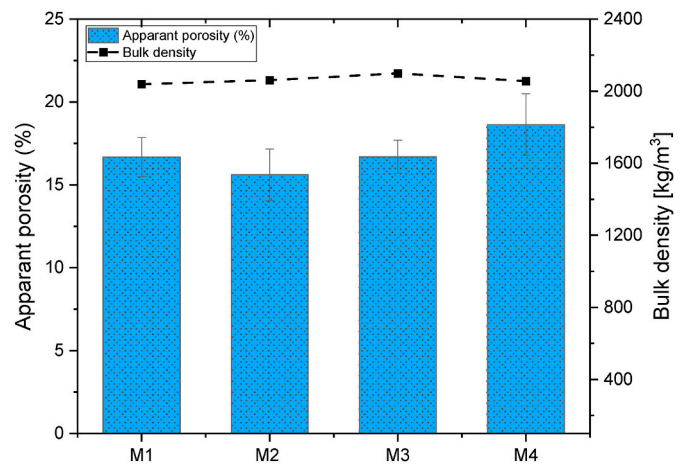


Fig. 12. Bulk density and apparent porosity values.

printed samples is found to be in the range of 15.6–18.7%. A similar range of porosity was also reported by past researchers for 3D-printed samples [42]. It is interesting to note that the trend of apparent porosity is similar to the compressive strength properties, where the  $M_2$  has the lowest apparent porosity and the  $M_4$  was the highest. Compared to the control mix ( $M_1$ ), the apparent porosity of the  $M_2$  mix decreased by 6.4%, the  $M_3$  showed the same apparent porosity and it was increased by 11.7% in  $M_4$ . This indicates that the small amount of brick waste replacement shows a micro-filling effect and reduces the porosity of printed specimens. In contrast, a higher level of replacement leads to large amounts of unreacted brick waste particles in the mix, which contributes to the porosity increment [17].

#### 4.3. Microstructural analysis of 3D printed concrete

The effect of brick waste incorporation on the micromorphological characteristics of 3D printed geopolymers is performed using the SEM analysis and the SEM images of 3D printed samples are shown in Fig. 13. According to the microstructure images, the  $M_1$  showed a dense and compacted microstructure and as the brick waste is introduced, a less dense and fragmented morphology with a higher amount of unreacted brick waste particles can be observed. This effect is more visible in the  $M_4$  type where the addition of brick waste is 50% of the total precursors. Moreover, the SEM images of the 3D printed samples also displayed some microcracks in all brick waste incorporated geopolymer mixes. This could be due to the elevated temperature curing at 60 °C, which could lead to cracks in the microstructures. A similar behaviour was also observed in the past by other researchers [57].

#### 4.4. Environmental impacts of the 3DCP with brick waste

The environmental impact of 3DCP with brick waste was quantified in terms of CO<sub>2</sub> emissions and energy consumption of various 3D printable mixes. The results are also compared with the conventional 3D printable concrete mix containing Ordinary Portland cement. To conduct this analysis, the carbon emissions and the embodied energy for the manufacturing of raw materials were obtained from the literature and are presented in Table 4. With the collected information for raw materials, the CO<sub>2</sub> emission and embodied energy for producing one cubic meter of 3D printable concrete mixes containing brick waste precursor is determined as depicted in Fig. 14. For comparison purposes, the corresponding information for conventional 3D printable mixes is also provided in the same figure.

The carbon emissions and embodied energy of 3D-printed concrete prepared with OPC with fly ash and slag were derived from published studies [62,67]. As can be seen in Fig. 14, regardless of the variation of brick waste content in 3D printable geopolymer mixes, the calculated

**Table 4**  
Carbon emission and embodied energy values of raw materials.

Raw materials	CO <sub>2</sub> emissions (kg/kg)	Embodied energy (MJ/kg)
Fly ash	0.02 [58]	0.05 [59]
Slag	0.0265 [58]	0.33 [36,60]
Brick waste	0.028 [61]	0.135 [61]
Cement	0.91 [62]	5.9 [62]
Sand	0.026 [36,63]	0.175 [36,63]
Sodium metasilicate	0.93 [36,64]	17.9 [36,64]
Retarder	0.307 [36,65]	0.822 [36,65]
Nano clay	1.5 [66]	40 [66]

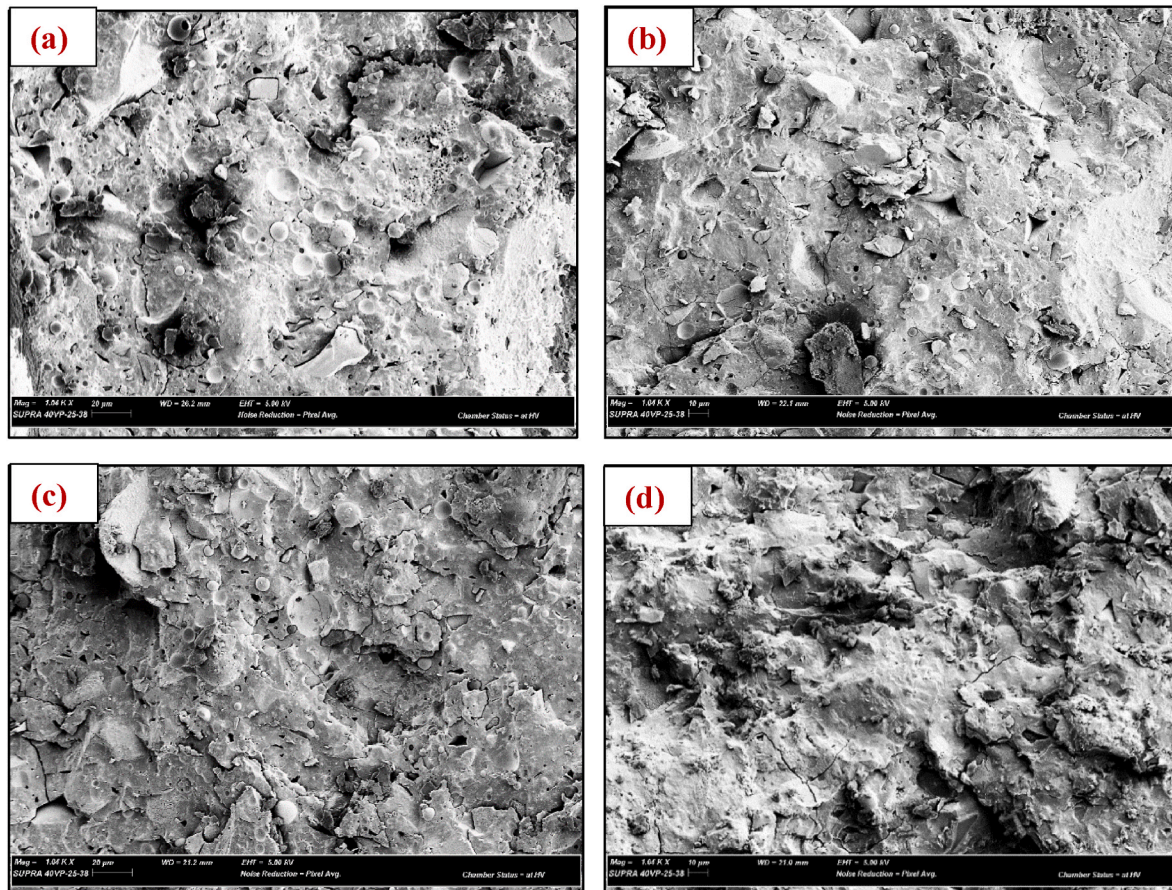


**Fig. 13.** SEM images of 3D printed geopolymer concrete, (a)  $M_1$ ; (b)  $M_2$ ; (c)  $M_3$ ; (d)  $M_4$ .

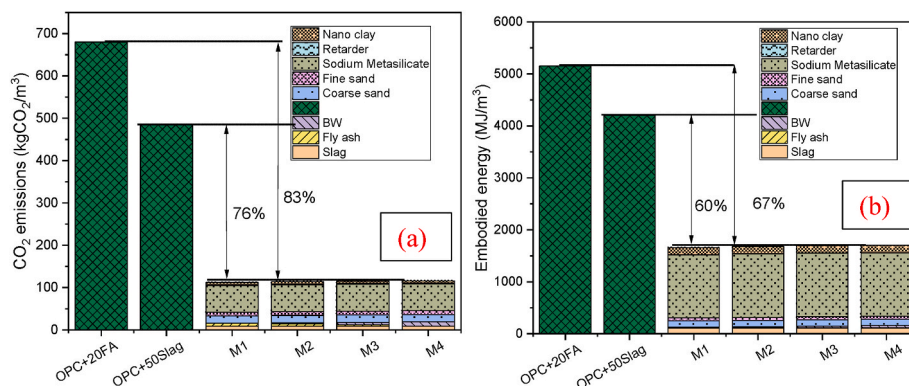


Fig. 14. (a) Carbon emission calculation, (b) Embodied energy calculation of 3D printed geopolymer concrete.

carbon emission of 3D printable geopolymer mixes is almost the same with a minor variation between the mixes. On the contrary, the conventional concrete with 20% fly ash mix (OPC+20FA) exhibits the highest carbon emission and the 3D printable OPC concrete mix with 50% slag substitution (OPC+50 slag) shows the second-highest carbon emission values. Compared to the OPC+20FA mix, the total carbon emission is reduced by 83% in the designated geopolymer mixes, whereas the corresponding reduction was observed between the (OPC+50 slag) mix and the geopolymer 3D printable mixes was 76%. Similarly, the total energy consumption of geopolymer 3D printable mixes was reduced by 67% and 60% compared to (OPC+20FA) and (OPC+50 slag) mixes respectively.

Considering the individual contribution of different ingredients for carbon emission and the energy consumption in 3D printable geopolymer mix, the activators are the main contributors in geopolymer concrete. In this study, 56% of total carbon emissions and 73% of energy consumption are associated with the activator component. Meanwhile, the precursor materials in 3D printable geopolymer mixes show 14% of carbon emission and 8% of total energy consumption for the M<sub>1</sub> mix (fly ash and slag) whereas, in M<sub>4</sub>, precursor materials (brick waste and slag) contributing 16% and 9% of total carbon emission and energy consumption, respectively. It should be noted that the CO<sub>2</sub> emissions and the energy consumption for the brick waste are associated with the demolition, collection and sorting, transportation, and recycling stages.

For (OPC+20FA) and (OPC+50Slag) mixes, more than 80% of total carbon emission and 50% of total energy consumption is associated with the Portland cement component [62,67]. This suggests that the use of Portland cement-based 3D printable mixes would still cause significant negative impacts, even though 3D printing has provided the benefits of reducing construction waste. On the other hand, in geopolymer 3D printable mixes, while the alkaline activators are contributing to a large portion of carbon emission and energy consumption, their proportion is very low. Therefore, the total carbon emission and energy consumption are significantly lower than Portland cement-based 3D printable concrete mixes.

Therefore, it can be concluded that geopolymer concrete is a sustainable alternative to OPC concrete for the 3D printing application, where the production of 3D printable geopolymer mixes exhibited a significant reduction in carbon emission and energy consumption. Besides, while the introduction of the brick waste precursor may not further reduce carbon emission or energy consumption, its utilization is additionally attributed to the environmental benefits of minimizing landfill waste and promoting the circular economy.

## 5. Conclusions

This paper investigated the feasibility of recycling the ground brick waste as a precursor for 3D printable geopolymer concrete in digital construction applications. The effects of the ground brick waste content

on the fresh and hardened properties of the geopolymer concrete suited for 3DCP were assessed. Based on the presented results, the following conclusions can be drawn:

- The increase in the brick waste content resulted in flowability losses in the mixes, whereas the setting time of the fresh mixes was increased with the brick waste in the mix.
- The rheological parameters such as apparent viscosity and static yield strength are increased with the brick waste content in the geopolymer mixes. This could be due to the loss of the ball-bearing effect and the high water absorption behaviour of brick waste in the mix.
- The anisotropic behaviour was observed in the compressive strength of 3D printed samples; the highest strength was reported in the printing direction, whereas the lowest strength was in the lateral direction.
- The compressive strength of 3D printable concrete is increased with the brick waste powder content by up to 10% with further increase in brick waste content leading to reduced compressive strength properties.
- The interlayer bond strength of the 3D printable geopolymer concrete also decreases with high brick waste content (above 10% of precursor content). For instance, the interlayer bond strength of M<sub>4</sub> (50% of brick waste in total precursor) has reduced by 16.8% at 28 days, compared to the control mix (M<sub>1</sub>).
- The embodied energy and carbon footprint of 3D printable geopolymer concrete reveals a 60–80% reduction compared to conventional Portland cement concrete, despite showing a minor variation within the various 3D printable geopolymers.

## Declaration of competing interest

The authors declare that they have no known competing financial interests or personal relationships that could have appeared to influence the work reported in this paper.

## Data availability

Data will be made available on request.

## Acknowledgement

The authors acknowledge the Swinburne University of Technology and the Australian Research Council (DE190100646) for supporting this work.

## References

- [1] Y. Zhang, et al., Rheological and harden properties of the high-thixotropy 3D printing concrete, *Construct. Build. Mater.* 201 (2019) 278–285.
- [2] M. Starr, World's first 3D-printed apartment building constructed in China. CNet [cited 2022 28-01-2022]; Available from: [www.cnet.com/news/worlds-first-3d-printed-apartment-building-constructed-in-china](http://www.cnet.com/news/worlds-first-3d-printed-apartment-building-constructed-in-china), 2015.
- [3] F. Bos, et al., Additive manufacturing of concrete in construction: potentials and challenges of 3D concrete printing, *Virtual Phys. Prototyp.* 11 (3) (2016) 209–225.
- [4] M. Sakin, Y.C. Kiroglu, 3D printing of buildings: construction of the sustainable houses of the future by BIM, *Energy Proc.* 134 (2017) 702–711.
- [5] G. Bai, et al., 3D printing eco-friendly concrete containing under-utilised and waste solids as aggregates, *Cement Concr. Compos.* 120 (2021), 104037.
- [6] W. Ferdous, et al., Recycling of landfill wastes (tyres, plastics and glass) in construction – a review on global waste generation, performance, application and future opportunities, *Resour. Conserv. Recycl.* 173 (2021), 105745.
- [7] P. J. C. Wardle, K. O'Farrell, P. Nyunt, S. Donovan, National Waste Report, Blue Environment prepared for Department of Agriculture, November 2020.
- [8] E. Australia, National waste report, Available from: <https://www.environment.gov.au/protection/waste/national-waste-reports/2020>, 2020.
- [9] P.B. Cachim, Mechanical properties of brick aggregate concrete, *Construct. Build. Mater.* 23 (3) (2009) 1292–1297.
- [10] C. Zheng, et al., Mechanical properties of recycled concrete with demolished waste concrete aggregate and clay brick aggregate, *Results Phys.* 9 (2018) 1317–1322.
- [11] K. Pasupathy, S. Ramakrishnan, J. Sanjayan, Effect of hydrophobic surface-modified fine aggregates on efflorescence control in geopolymer, *Cement Concr. Compos.* (2021), 104337.
- [12] I. Diaz-Loya, et al., Extending supplementary cementitious material resources: reclaimed and remediated fly ash and natural pozzolans, *Cement Concr. Compos.* 101 (2019) 44–51.
- [13] M.J. Tapas, et al., Comparative study of the efficacy of fly ash and reactive aggregate powders in mitigating alkali-silica reaction, *J. Build. Eng.* 63 (2023), 105571.
- [14] C.L. Wong, et al., Mechanical strength and permeation properties of high calcium fly ash-based geopolymer containing recycled brick powder, *J. Build. Eng.* (2020), 101655.
- [15] P. Rownan'k, et al., Rheological properties and microstructure of binary waste red brick powder/metakaolin geopolymer, *Construct. Build. Mater.* 188 (2018) 924–933.
- [16] L. Reig, et al., Properties and microstructure of alkali-activated red clay brick waste, *Construct. Build. Mater.* 43 (2013) 98–106.
- [17] K. Pasupathy, S. Ramakrishnan, J. Sanjayan, Formulating eco-friendly geopolymer foam concrete by alkali-activation of ground brick waste, *J. Clean. Prod.* 325 (2021), 129180.
- [18] D. Yang, M. Liu, Z. Ma, Properties of the foam concrete containing waste brick powder derived from construction and demolition waste, *J. Build. Eng.* 32 (2020), 101509.
- [19] J. Migunthanna, P. Rajeev, J. Sanjayan, Investigation of waste clay brick as partial replacement of geopolymer binders for rigid pavement application, *Construct. Build. Mater.* 305 (2021), 124787.
- [20] I. Demir, H. Yaprak, O. Simsek, Performance of cement mortars replaced by ground waste brick in different aggressive conditions, *Ceramics* 55 (3) (2011) 268–275.
- [21] R. Toledo Filho, et al., Potential for use of crushed waste calcined-clay brick as a supplementary cementitious material in Brazil, *Cement Concr. Res.* 37 (9) (2007) 1357–1365.
- [22] M.S. Kirgiz, Strength gain mechanisms of blended-cements containing marble powder and brick powder, *KSCCE J. Civ. Eng.* 19 (1) (2015) 165–172.
- [23] Y. Zhao, et al., The particle-size effect of waste clay brick powder on its pozzolanic activity and properties of blended cement, *J. Clean. Prod.* 242 (2020), 118521.
- [24] K. Pasupathy, S. Ramakrishnan, J. Sanjayan, Enhancing the properties of foam concrete 3D printing using porous aggregates, *Cement Concr. Compos.* 133 (2022), 104687.
- [25] J. Zhang, et al., A review of the current progress and application of 3D printed concrete, *Compos. Appl. Sci. Manuf.* 125 (2019), 105533.
- [26] M.K. Mohan, et al., Extrusion-based concrete 3D printing from a material perspective: a state-of-the-art review, *Cement Concr. Compos.* 115 (2021), 103855.
- [27] T.D. Ngo, et al., Additive manufacturing (3D printing): a review of materials, methods, applications and challenges, *Compos. B Eng.* 143 (2018) 172–196.
- [28] T. Ding, et al., Hardened properties of layered 3D printed concrete with recycled sand, *Cement Concr. Compos.* 113 (2020), 103724.
- [29] Y. Wu, et al., Study on the rheology and buildability of 3D printed concrete with recycled coarse aggregates, *J. Build. Eng.* 42 (2021), 103030.
- [30] J. Liu, et al., 3D-printed concrete with recycled glass: effect of glass gradation on flexural strength and microstructure, *Construct. Build. Mater.* 314 (2022), 125561.
- [31] M. Sambucci, M. Valente, Influence of waste tire rubber particles size on the microstructural, mechanical, and acoustic insulation properties of 3D-printable cement mortars, *Civil Eng. J.* 7 (2021), 06.
- [32] Z. Duan, et al., Rheological properties of mortar containing recycled powders from construction and demolition wastes, *Construct. Build. Mater.* 237 (2020), 117622.
- [33] A.S.N. Zealand, Committee BD-031, Supplementary cementitious materials Part 1: fly ash, in *AS/NZS 3582 1*, 2016, 2016.
- [34] S.H. Bong, et al., Efficiency of different superplasticizers and retarders on properties of 'one-Part' Fly ash-slag blended geopolymers with different activators, *Materials* 12 (20) (2019) 3410.
- [35] S. Muthukrishnan, S. Ramakrishnan, J. Sanjayan, Effect of alkali reactions on the rheology of one-part 3D printable geopolymer concrete, *Cement Concr. Compos.* 116 (2021), 103899.
- [36] S.H. Bong, et al., Ambient temperature cured 'just-add-water' geopolymer for 3D concrete printing applications, *Cement Concr. Compos.* 121 (2021), 104060.
- [37] B. Panda, et al., Synthesis and characterization of one-part geopolymers for extrusion based 3D concrete printing, *J. Clean. Prod.* 220 (2019) 610–619.
- [38] S.H. Bong, et al., Properties of one-part geopolymer incorporating wollastonite as partial replacement of geopolymer precursor or sand, *Mater. Lett.* 263 (2020), 127236.
- [39] M. Xia, J.G. Sanjayan, Methods of enhancing strength of geopolymer produced from powder-based 3D printing process, *Mater. Lett.* 227 (2018) 281–283.
- [40] Y.W.D. Tay, Y. Qian, M.J. Tan, Printability region for 3D concrete printing using slump and slump flow test, *Compos. B Eng.* 174 (2019), 106968.
- [41] A. C. Standard Test Method for Flow of Hydraulic Cement Mortar, 2001. Philadelphia, PA.
- [42] S. Ramakrishnan, et al., Concrete 3D printing of lightweight elements using hollow-core extrusion of filaments, *Cement Concr. Compos.* 123 (2021), 104220.
- [43] A. ASTM, c191-13 Standard Test Methods for Time of Setting of Hydraulic Cement by Vicat Needle, ASTM International, West Conshohocken, PA, USA, 2013.
- [44] T. Marchment, J. Sanjayan, M. Xia, Method of enhancing interlayer bond strength in construction scale 3D printing with mortar by effective bond area amplification, *Mater. Des.* 169 (2019), 107684.
- [45] Q. Tang, et al., The utilization of eco-friendly recycled powder from concrete and brick waste in new concrete: a critical review, *Cement Concr. Compos.* 114 (2020), 103807.
- [46] M. Chen, et al., Yield stress and thixotropy control of 3D-printed calcium sulfoaluminate cement composites with metakaolin related to structural build-up, *Construct. Build. Mater.* 252 (2020), 119090.
- [47] C. Liu, et al., Influence of hydroxypropyl methylcellulose and silica fume on stability, rheological properties, and printability of 3D printing foam concrete, *Cement Concr. Compos.* 122 (2021), 104158.
- [48] M. Chen, et al., Rheological parameters, thixotropy and creep of 3D-printed calcium sulfoaluminate cement composites modified by bentonite, *Compos. B Eng.* 186 (2020), 107821.
- [49] M. Tuyan, Ö. Andiç-Çakir, K. Ramyar, Effect of alkali activator concentration and curing condition on strength and microstructure of waste clay brick powder-based geopolymer, *Compos. B Eng.* 135 (2018) 242–252.
- [50] G.H.A. Ting, Y.W.D. Tay, M.J. Tan, Experimental measurement on the effects of recycled glass cullets as aggregates for construction 3D printing, *J. Clean. Prod.* 300 (2021), 126919.
- [51] T.T. Le, et al., Hardened properties of high-performance printing concrete, *Cement Concr. Res.* 42 (3) (2012) 558–566.
- [52] D. Asprone, et al., Rethinking reinforcement for digital fabrication with concrete, *Cement Concr. Res.* 112 (2018) 111–121.
- [53] M. van den Heever, et al., Evaluating the effects of porosity on the mechanical properties of extrusion-based 3D printed concrete, *Cement Concr. Res.* 153 (2022), 106695.
- [54] E. Keita, et al., Weak bond strength between successive layers in extrusion-based additive manufacturing: measurement and physical origin, *Cement Concr. Res.* 123 (2019), 105787.
- [55] G. Ma, et al., Mechanical characterization of 3D printed anisotropic cementitious material by the electromechanical transducer, *Smart Mater. Struct.* 27 (7) (2018), 075036.
- [56] S. Yu, et al., Microstructural characterization of 3D printed concrete, *J. Build. Eng.* 44 (2021), 102948.
- [57] J. Fort, et al., Characterization of geopolymers prepared using powdered brick, *J. Mater. Res. Technol.* 8 (6) (2019) 6253–6261.
- [58] K.-H. Yang, J.-K. Song, K.-I. Song, Assessment of CO<sub>2</sub> reduction of alkali-activated concrete, *J. Clean. Prod.* 39 (2013) 265–272.
- [59] E. Jamieson, et al., Comparison of embodied energies of ordinary Portland cement with byer-derived geopolymer products, *J. Clean. Prod.* 99 (2015) 112–118.
- [60] G. Habert, J.D.E. De Lacaillerie, N. Roussel, An environmental evaluation of geopolymer based concrete production: reviewing current research trends, *J. Clean. Prod.* 19 (11) (2011) 1229–1238.
- [61] J. Fort, et al., Application of waste brick powder in alkali activated aluminosilicates: functional and environmental aspects, *J. Clean. Prod.* 194 (2018) 714–725.
- [62] S. Bhattacherjee, et al., Sustainable materials for 3D concrete printing, *Cement Concr. Compos.* 122 (2021), 104156.
- [63] E.-H. Yang, Y. Yang, V.C. Li, Use of high volumes of fly ash to improve ECC mechanical properties and material greenness, *ACI Mater. J.* 104 (6) (2007) 620.
- [64] M. Fawer, M. Concannon, W. Rieber, Life cycle inventories for the production of sodium silicates, *Int. J. Life Cycle Assess.* 4 (4) (1999) 207.
- [65] P. Rein, The carbon footprint of sugar, *Proc. Int. Soc. Sugar Cane Technol.* 27 (2010) 15.
- [66] D. LeCorre, et al., Comparative sustainability assessment of starch nanocrystals, *J. Polym. Environ.* 21 (1) (2013) 71–80.
- [67] A. Rahul, A. Sharma, M. Santhanam, A desorptivity-based approach for the assessment of phase separation during extrusion of cementitious materials, *Cement Concr. Compos.* 108 (2020), 103546.